

## Measurement of $D^*$ meson production in deep inelastic $ep$ scattering at low $Q^2$

ZEUS Collaboration

### Abstract

The production of  $D^*(2010)$  mesons in deep inelastic scattering at low  $Q^2$  has been measured with the ZEUS detector at HERA using an integrated luminosity of  $81.9 \text{ pb}^{-1}$ . The decay channel  $D^{*+} \rightarrow D^0 \pi^+$  with  $D^0 \rightarrow K^- \pi^+$  and corresponding antiparticle decay were used to identify  $D^*$  mesons. Using the beam-pipe calorimeter of ZEUS, differential  $D^*$  cross sections as functions of exchanged photon virtuality,  $Q^2$ , inelasticity,  $y$ , transverse momentum of the  $D^*$  meson,  $p_T(D^*)$ , and pseudorapidity of the  $D^*$  meson,  $\eta(D^*)$ , have been measured. The kinematic region of the measurement is  $0.05 < Q^2 < 0.7 \text{ GeV}^2$ ,  $0.02 < y < 0.85$ ,  $1.5 < p_T(D^*) < 9.0 \text{ GeV}$  and  $|\eta(D^*)| < 1.5$ . The measured differential cross sections are well described by predictions of next-to-leading-order QCD.



# 1 Introduction

Charm quarks in photoproduction and deep inelastic scattering (DIS) have been extensively studied at HERA [1–6]. These measurements are consistent with perturbative QCD calculations indicating boson-gluon fusion (BGF) as the dominant mechanism of charm production. For most of the charm DIS measurements  $D^*$  mesons are selected and the  $Q^2$  region is restricted to values above 1.5 GeV<sup>2</sup>.

Measurements of charm production in DIS at low  $Q^2$  are presented in this paper. By selecting  $D^*$  mesons for  $0.05 < Q^2 < 0.7$  GeV<sup>2</sup>, the transition region from DIS to photoproduction is probed. This measurement was performed using the beam pipe calorimeter (BPC) [7,8]. Differential cross sections have been measured as a function of  $Q^2$ ,  $y$ ,  $p_T(D^*)$  and  $\eta(D^*)$  and compared to NLO predictions using the HVQDIS program.

## 2 Experimental set-up

The data presented in this analysis were collected with the ZEUS detector at HERA during the 1998-2000 running periods, with  $e^\pm$  beam energy of  $E_e = 27.5$  GeV colliding with a proton beam energy of  $E_p = 920$  GeV. The data sample corresponds to an integrated luminosity of 82 pb<sup>-1</sup>.

A detailed description of the ZEUS detector can be found elsewhere [9]. A brief outline of the components that are most relevant for this analysis is given below.

Charged particles are tracked in the central tracking detector (CTD) [10], which operates in a magnetic field of 1.43 T provided by a thin superconducting solenoid. The CTD consists of 72 cylindrical drift chamber layers, organised in nine superlayers covering the polar-angle<sup>1</sup> region  $15^\circ < \theta < 164^\circ$ . The transverse-momentum resolution for full-length tracks is  $\sigma(p_T)/p_T = 0.0058p_T \oplus 0.0065 \oplus 0.0014/p_T$ , with  $p_T$  in GeV.

The high-resolution uranium-scintillator calorimeter (CAL) [11] consists of three parts: the forward, the barrel and the rear calorimeters. The smallest subdivision of the calorimeter is called a cell. The CAL energy resolutions, as measured under test-beam conditions, are  $\sigma(E)/E = 0.18/\sqrt{E}$  for electrons and  $\sigma(E)/E = 0.35/\sqrt{E}$  for hadrons, with  $E$  in GeV.

The BPC is a small calorimeter designed to provide an accurate measurement of the energy and position of the electron at very small scattering angles. The detector covers

---

<sup>1</sup> The ZEUS coordinate system is a right-handed Cartesian system, with the  $Z$  axis pointing in the proton beam direction, referred to as the “forward direction”, and the  $X$  axis pointing left towards the centre of HERA. The coordinate origin is at the nominal interaction point.

the range  $0.045 < Q^2 < 0.7 \text{ GeV}^2$ . There are 2 BPC modules installed – north and south. The north BPC is used for physics analysis and will be denoted as BPC. The south BPC module has a substantially reduced active area and is therefore used only for alignment and calibration. The BPC consists of 36 layers of 3.5 mm thick tungsten alloy absorber planes interleaved with 2.6 mm thick scintillator strips. It is about  $24X_0$  along  $z$  ( $\sim 16 \text{ cm}$ ). The energy resolution of the BPC is  $\sigma(E)/E \sim 17\%/\sqrt{E}$ , with  $E$  in GeV.

### 3 $D^*$ production at low $Q^2$

#### 3.1 Event selection

Events which fulfil the following conditions were selected: characteristic energy deposit of an electron within the fiducial area of the BPC with  $E_{\text{BPC}} > 4 \text{ GeV}$ ; BPC timing measurement consistent with an  $ep$  interaction  $|\langle \tau_{\text{BPC}} \rangle| < 3 \text{ ms}$ ; a primary vertex with  $|Z_{\text{vertex}}| < 50 \text{ cm}$  was reconstructed; the ratio of the transverse momentum of the  $D^*$  to the total transverse CAL energy deposit was  $p_T(D^*)/E_T > 0.1$  and  $35 < \delta_{\text{BPC}} < 65 \text{ GeV}$ , where  $\delta_{\text{BPC}} = \delta + E_{\text{BPC}}(1 - \cos(\Theta_{\text{BPC}}))$ ,  $\delta = \sum_i (E - p_z)_i$ , and the index  $i$  runs over the CAL clusters and  $\Theta_{\text{BPC}}$  is the angle of the scattered electron w.r.t. the proton beam axis. Events with an additional reconstructed electron in the calorimeter are suppressed.

The selected kinematic region was  $0.05 < Q^2 < 0.7 \text{ GeV}^2$  and  $0.02 < y < 0.85$ .

#### 3.2 Reconstruction of $D^*$ mesons

The  $D^*$  mesons were reconstructed from the decay channels  $D^{*+} \rightarrow D^0 \pi_s^+$  (+c.c.) with  $D^0 \rightarrow K^- \pi^+$  (+c.c.). In each event, pairs of tracks with  $p_T > 0.45 \text{ GeV}$  were combined to form a  $D^0$  candidate. A third track with  $p_T > 0.12 \text{ GeV}$  and charge opposite to that of the kaon track was combined with the  $D^0$  candidate to form a  $D^*$  candidate, and kept if its charge was opposite to the kaon track. A different mass window for the  $D^0$  was used for each bin of  $p_T(D^*)$ :  $1.82 < M(K\pi) < 1.91 \text{ GeV}$ ,  $1.81 < M(K\pi) < 1.92 \text{ GeV}$ ,  $1.80 < M(K\pi) < 1.93 \text{ GeV}$  and  $1.79 < M(K\pi) < 1.94 \text{ GeV}$  for  $1.5 < p_T(D^*) < 3.25 \text{ GeV}$ ,  $3.25 < p_T(D^*) < 5 \text{ GeV}$ ,  $5 < p_T(D^*) < 8 \text{ GeV}$  and  $8 < p_T(D^*) < 9 \text{ GeV}$ , respectively.

$D^*$  mesons were selected in the kinematic region  $1.5 < p_T(D^*) < 9 \text{ GeV}$  and  $|\eta(D^*)| < 1.5$ .

Figure 1 shows the  $\Delta M$  distribution measured with a electron reconstructed in the BPC. A clear signal is seen around the nominal value of  $M(D^*) - M(D^0)$ . The number of  $D^*$  mesons, extracted by an unbinned fit, was  $N(D^*) = 253 \pm 25$ .

### 3.3 Cross sections

The inclusive  $D^*$  cross sections at low  $Q^2$  were measured in the kinematic region  $0.05 < Q^2 < 0.7 \text{ GeV}^2$ ,  $0.02 < y < 0.85$ ,  $1.5 < p_T(D^*) < 9 \text{ GeV}$  and  $|\eta(D^*)| < 1.5$ . The HERWIG [12] Monte Carlo program was used to correct the data for detector effects and calculate acceptances. The measured cross section is

$$\sigma(e^\pm p \rightarrow e^\pm D^* X) = 10.1 \pm 1.0(\text{stat})_{-0.8}^{+1.1}(\text{syst}) \text{ nb.}$$

The replacement of HERWIG by RAPGAP for acceptance corrections was the main source of systematic error.

Figures 2-5 show the single differential cross sections as a function of  $Q^2$ ,  $y$ ,  $p_T(D^*)$  and  $\eta(D^*)$  compared to the NLO QCD predictions. In general, shape and normalization of the distributions are described by the NLO predictions. A comparison of  $d\sigma/dQ^2$  with previous ZEUS results is shown in figure 6. For this figure, in order to have data comparable to older measurements, the  $y$  range was restricted to  $0.02 < y < 0.7$ . The unbinned fit in this restricted kinematic region yielded  $N(D^*) = 239 \pm 23$ .

### 3.4 NLO QCD predictions

The NLO prediction of the  $c\bar{c}$  cross section was obtained using the program HVQDIS. At low  $Q^2$ , HVQDIS is applicable because the calculation neglects terms of orders higher than  $\alpha_s^2$ . These terms contain  $\log(Q^2/m_c^2)$  factors which can become large for  $Q^2 \gg m_c^2$ . Therefore, the HVQDIS results are expected to be more accurate at  $Q^2 \approx m_c^2$ . The fragmentation of the charm quarks was performed according to the Peterson model with the parameter  $\epsilon = 0.035$ . The nominal mass of the charm quark was set to  $m_c = 1.35 \text{ GeV}$ . The normalisation and factorisation scales were set to  $\mu = \sqrt{Q^2 + 4m_c^2}$ . The ZEUS NLO QCD fit and CTEQ5F3 were used as the parametrisation of the proton PDFs. The NLO predicted total cross section is

$$\sigma_{\text{HVQDIS}}(e^\pm p \rightarrow e^\pm D^* X) = 8.6_{-1.8}^{+1.9}(\text{syst.}) \text{ nb}$$

To estimate the theoretical uncertainty, the ZEUS PDF fit [13] was used and the scale  $\mu$ , the mass of the charm quark and the parameter  $\epsilon$  in the Peterson fragmentation function were varied in the range:  $(Q^2 + m_c^2) < \mu^2 < 4(Q^2 + 4m_c^2)$ ,  $1.2 < m_c < 1.5 \text{ GeV}$ ,  $0.02 < \epsilon < 0.05$ , respectively. The mass variation is the dominant source of uncertainty.

## 4 Summary

The production of  $D^*$  mesons in DIS at HERA was measured with the ZEUS detector in the kinematic region  $0.05 < Q^2 < 0.7 \text{ GeV}^2$ ,  $0.02 < y < 0.85$ ,  $1.5 < p_T(D^*) < 9 \text{ GeV}$ ,  $|\eta(D^*)| < 1.5$ , probing the transition region to photoproduction regime. The theoretical NLO QCD calculation of BGF charm production is consistent with the measured cross sections at low  $Q^2$ .

## References

- [1] ZEUS Coll., S. Chekanov et al., Phys. Rev. **D 69**, 0120004 (2004).
- [2] H1 Coll., C. Adloff et al., Phys. Lett. **B 528**, 199 (2002).
- [3] ZEUS Coll., J. Breitweg et al., Phys. Lett. **B 481**, 213 (2000).
- [4] ZEUS Coll., J. Breitweg et al., Eur. Phys. J. **C 12**, 35 (2000).
- [5] H1 Coll., C. Adloff et al., Nucl. Phys. **B 545**, 21 (1999).
- [6] ZEUS Coll., J. Breitweg et al., Eur. Phys. J. **C 6**, 67 (1999).
- [7] C. Amelung, *Measurement of the Proton Structure Function  $F_2$  at Very Low  $Q^2$  at HERA*. Ph.D. Thesis, Universität Bonn, Bonn, (Germany), Report BONN-IR-99-14, DESY-THESIS-2000-002, 1999.
- [8] B. Surrow, *Measurement of the proton structure function  $F_2$  at low  $Q^2$  and very low  $x$  with the ZEUS beam pipe calorimeter at HERA*. Ph.D. Thesis, Hamburg University, Report DESY-THESIS-1998-004, 1998.
- [9] ZEUS Coll., U. Holm (ed.), *The ZEUS Detector*. Status Report (unpublished), DESY (1993), available on <http://www-zeus.desy.de/bluebook/bluebook.html>.
- [10] N. Harnew et al., Nucl. Inst. Meth. **A 279**, 290 (1989);  
B. Foster et al., Nucl. Phys. Proc. Suppl. **B 32**, 181 (1993);  
B. Foster et al., Nucl. Inst. Meth. **A 338**, 254 (1994).
- [11] M. Derrick et al., Nucl. Inst. Meth. **A 309**, 77 (1991);  
A. Andresen et al., Nucl. Inst. Meth. **A 309**, 101 (1991);  
A. Caldwell et al., Nucl. Inst. Meth. **A 321**, 356 (1992);  
A. Bernstein et al., Nucl. Inst. Meth. **A 336**, 23 (1993).
- [12] G. Marchesini et al., Comp. Phys. Comm. **67**, 465 (1992).
- [13] ZEUS Coll., S. Chekanov et al., Phys. Rev. **D 67**, 012007 (2003).

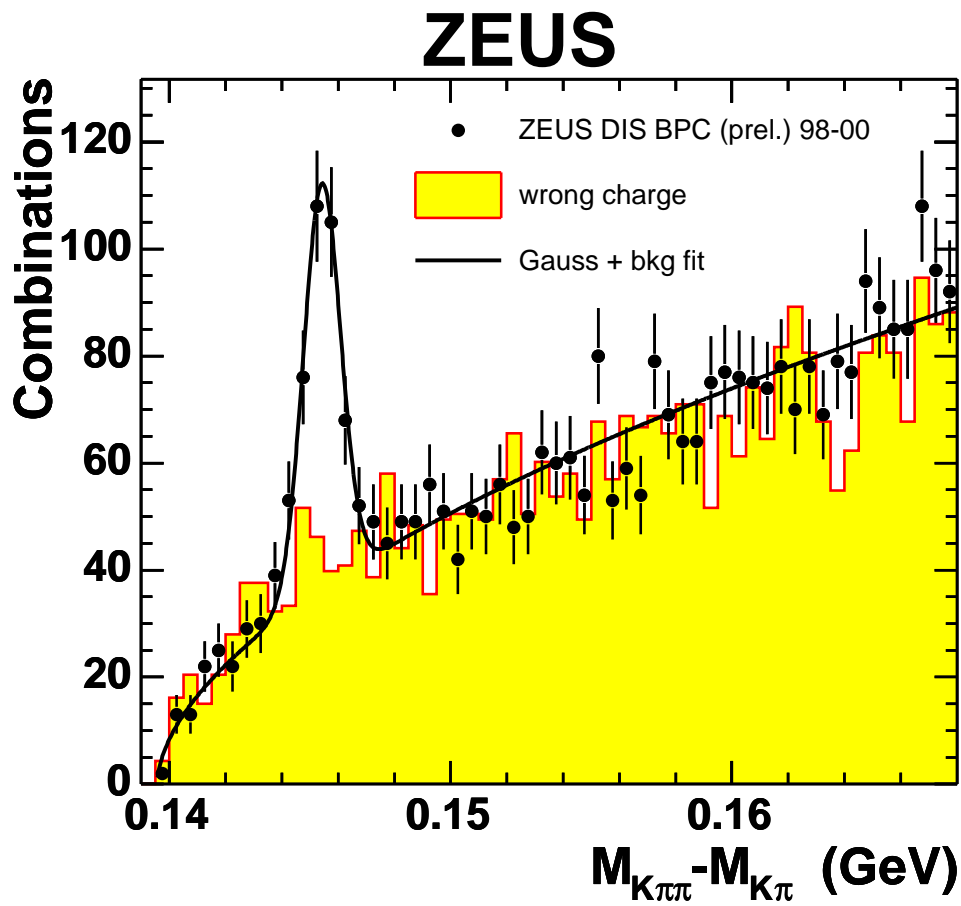


**Figure 1:** *The distribution of the mass difference,  $\Delta M = M(K\pi\pi_s) - M(K\pi)$ , for  $D^{*\pm}$  candidates from BPC measurements. The histogram shows the  $\Delta M$  distribution for wrong charge combinations. The solid curve represents the fit.*

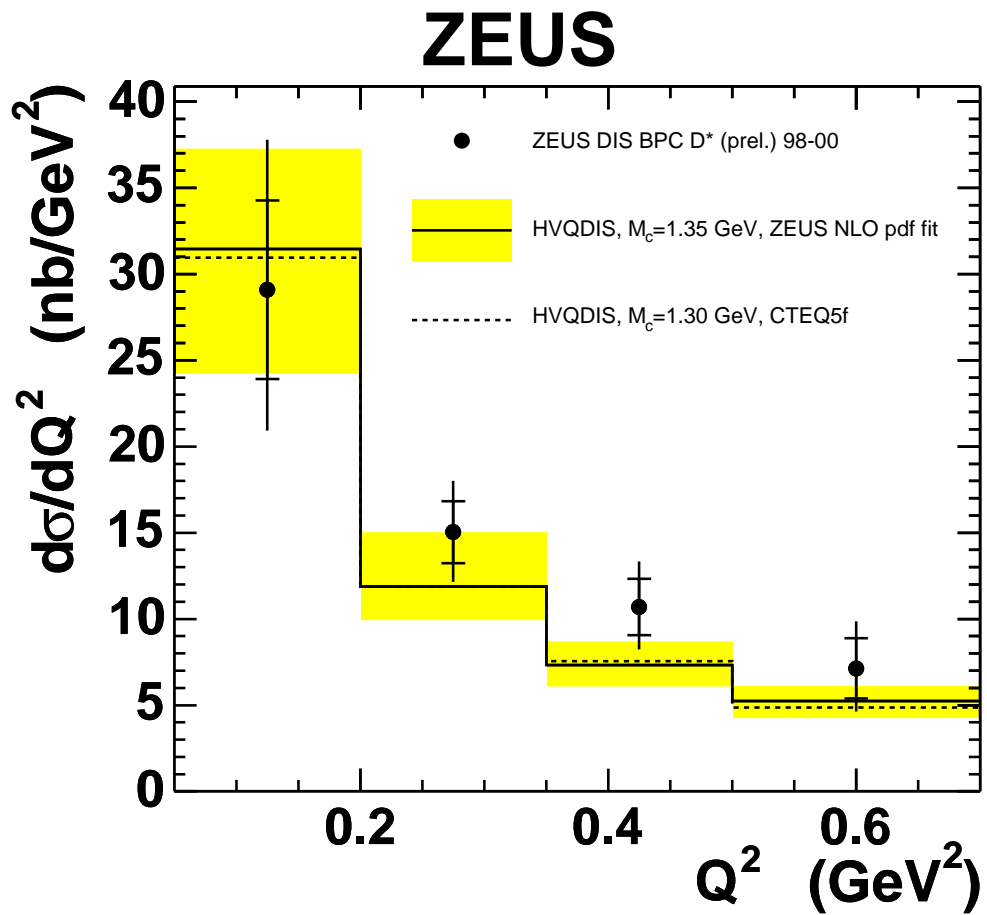


**Figure 2:** *Differential  $D^*$  cross sections as a function of  $Q^2$  compared to the NLO predictions of HVQDIS.*

# ZEUS

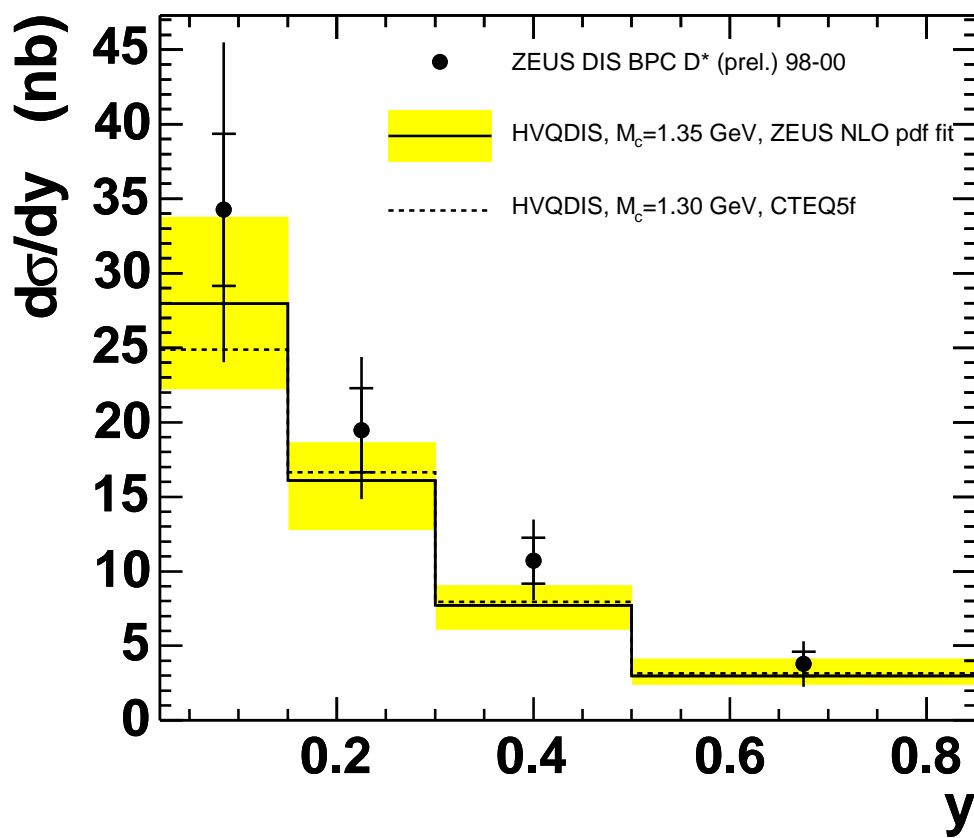


**Figure 3:** *Differential  $D^*$  cross sections as a function of  $y$  compared to the NLO predictions of HVQDIS.*

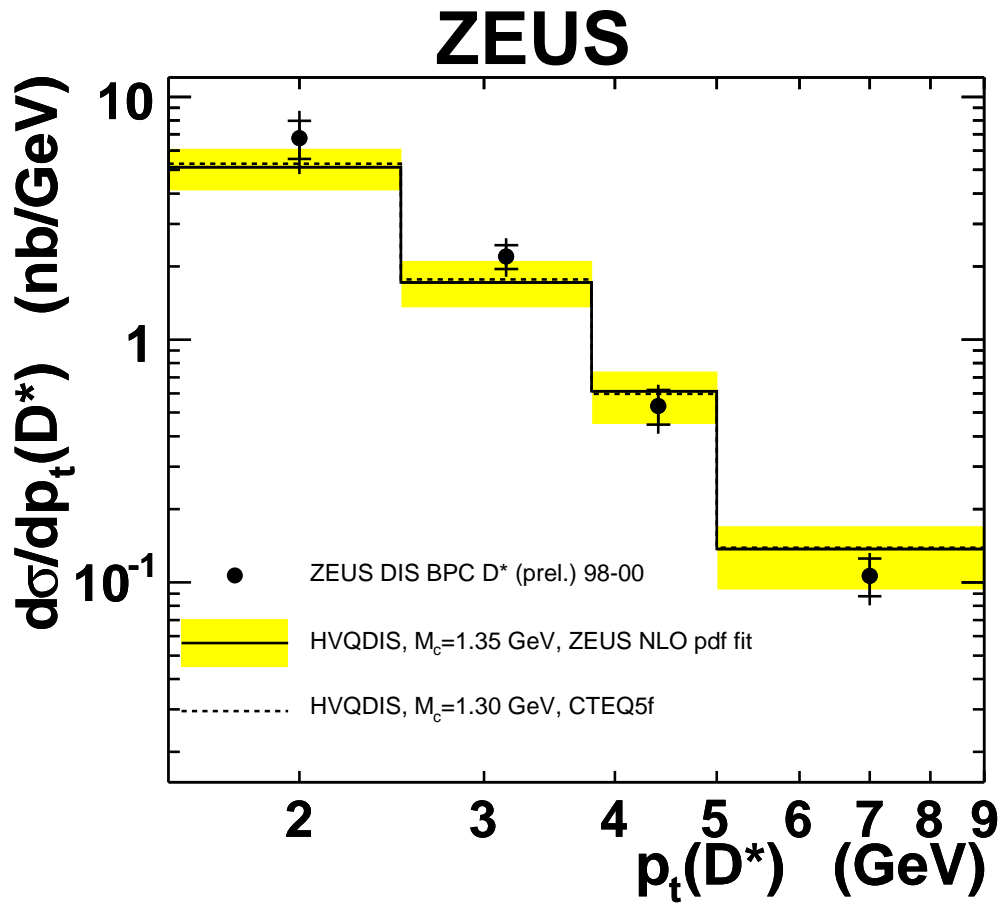


**Figure 4:** *Differential  $D^*$  cross sections as a function of  $p_T(D^*)$  compared to the NLO predictions of HVQDIS.*

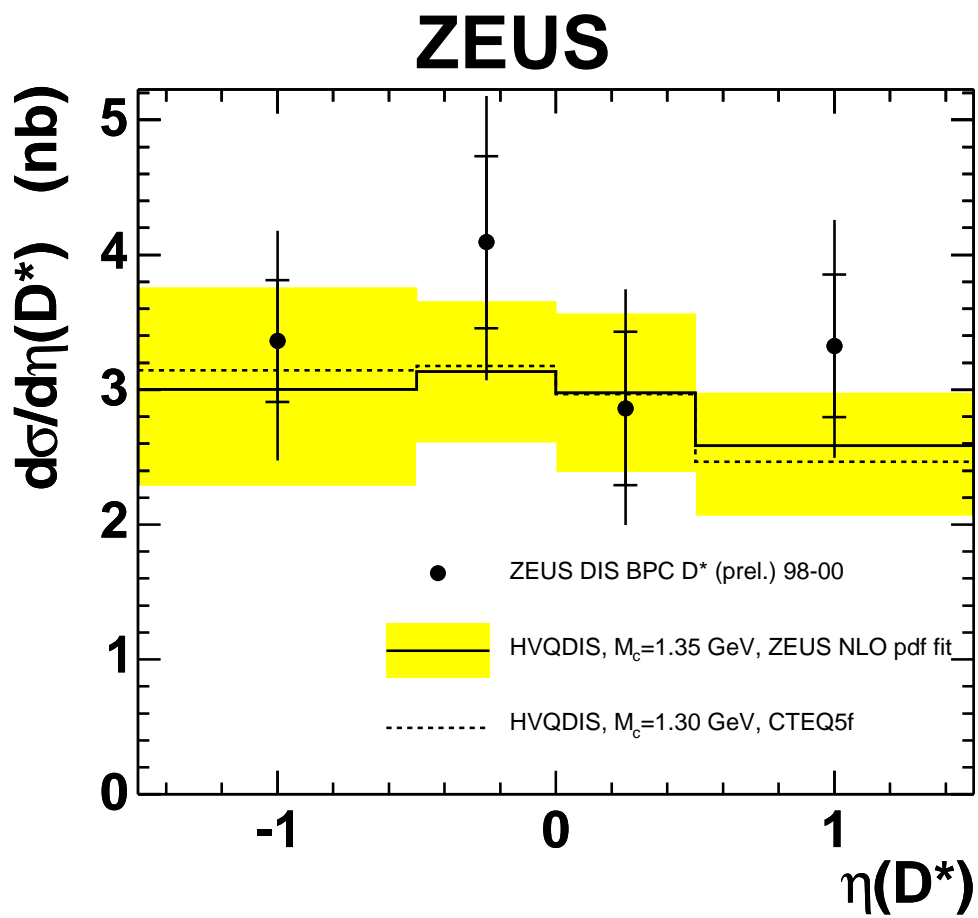


**Figure 5:** *Differential  $D^*$  cross sections as a function of  $\eta(D^*)$  compared to the NLO predictions of HVQDIS.*

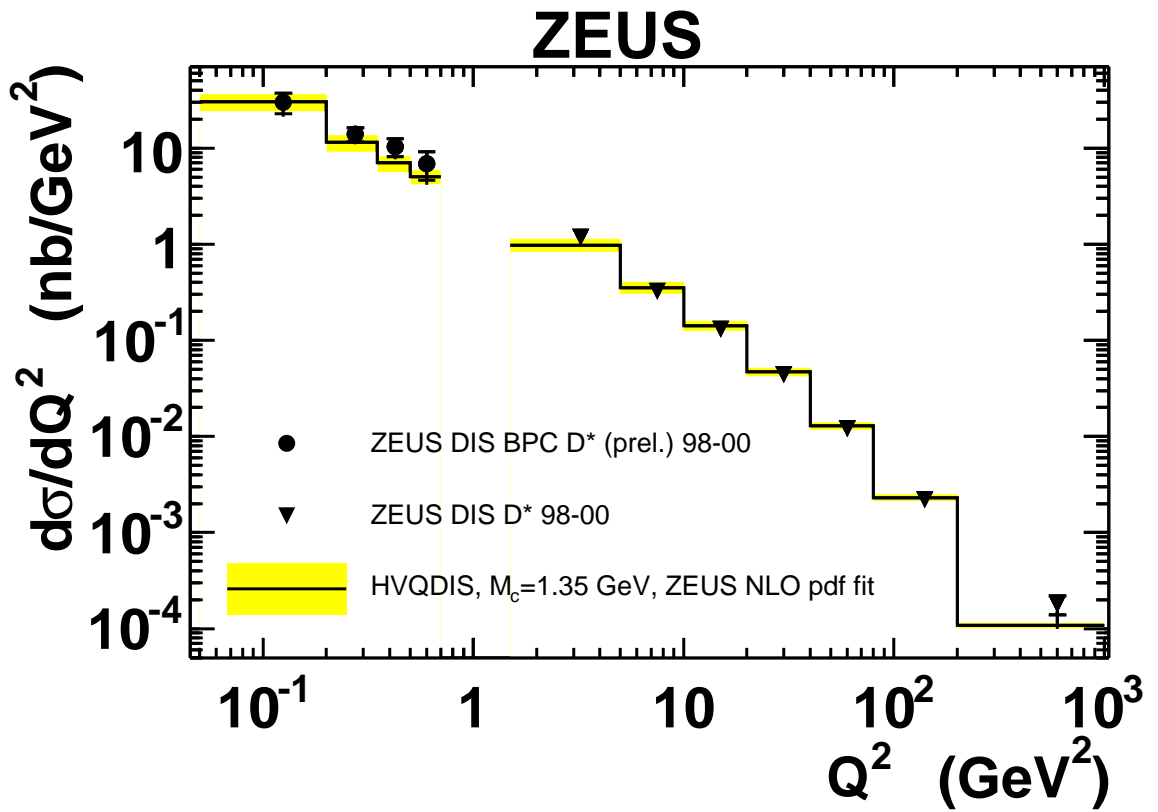


**Figure 6:** *Differential  $D^*$  cross sections as a function of  $Q^2$  for low  $Q^2$  and from previous results on  $D^*$  production in DIS compared to the NLO predictions from HVQDIS.*